Quantum Electromagnetic Transients Program

Yifan Zhou, *Member, IEEE*, Fei Feng, *Student Member, IEEE*, and Peng Zhang, *Senior Member, IEEE*

***Abstract*—This letter devises a quantum electromagnetic transients program (QEMTP) which is the first attempt to tackle the computational challenges in solving EMTP through quantum computing. The main contributions lie in: (1) A quantum-enabled EMTP formulation with Dommel's model encoded in quantum states; 2) An Harrow-Hassidim-Lloyd (HHL)-based QEMTP to solve the discrete-time nodal equations; 3) An iteration-based HHL revision for mitigating temporal errors to achieve high accuracy of QEMTP with limited quantum resources. Case studies verify the correctness and efficacy of QEMTP in simulating both fast and slow dynamics.**

***Index Terms*—Power system dynamics, quantum electromagnetic transients program (QEMTP), quantum computing.**

I. Introduction

ELECTROMAGNETIC transients program (EMTP) is a fundamentally important tool capable of providing complete and accurate information of electromagnetic dynamics, including spectra centered around DC and fundamental frequency up to ultra-high frequency transients [1]. In recent years, the necessity of using EMTP in system planning and operations swiftly grows with the ever-increasing integration of power electronics devices and variable distributed energy resources.

Solving EMTP remains to be a formidable problem even on the powerful and expensive real-time simulators such as RTDS [2]. The curse of dimensionality makes existing EMTP algorithms unscalable and unable to offer real-time, high-fidelity results needed for managing massive electronic devises and ensuring resilient power system operations.

Recent breakthroughs in quantum computing shed lights on a 'quantum leap' of EMTP solutions. While the complexity of numerical integration (i.e., the core of EMTP) on classical computers scales polynomially with the problem size, the quantum computer attains a logarithmically-growing computational complexity [3]. Thus, a quantum computing empowered EMTP, previously nonexistent, is promising to achieve an exponential speedup over today's EMTP tools.

This letter is the first attempt to bridge the gap between classical and quantum EMTP approaches. Major innovations of Quantum EMTP (QEMTP) include: 1) a quantum-encoded EMTP formulation; 2) an Harrow-Hassidim-Lloyd (HHL) algorithm [4] based EMTP solver; and 3) a practical revision of HHL with an error compensation technique for improving accuracy. The proof-of-concept of QEMTP under various transients scenarios verifies its accuracy and efficacy.

II. Quantum EMTP Formulation

A. Classical EMTP Formulation

Classical EMTP formulation in the matrix form can be established as [1]:

$$\boldsymbol{G}_0\boldsymbol{v}(t) = \boldsymbol{i}_s(t) + \boldsymbol{i}_h(t) := \boldsymbol{i}(t) \tag{1}$$

Here, $\boldsymbol{v}$ denotes the vector of nodal voltages; $\boldsymbol{i}_s$ denotes the vector of current sources; $\boldsymbol{i}_h$ denotes the vector of "history" terms; $\boldsymbol{i}$ denotes the vector of "assembled" nodal current injections including current sources and history terms; $\boldsymbol{G}_0$ is the equivalent conductance matrix of dimension N.

B. Quantum EMTP Formulation

Reformulating (1) into a quantum representation leads to:

$$\boldsymbol{G}|\boldsymbol{v}\rangle = |\boldsymbol{i}\rangle \tag{2}$$

Here, $\boldsymbol{G}$ is a rescaled unit-determinant matrix of $\boldsymbol{G}_0$; $|\boldsymbol{v}\rangle$ and $|\boldsymbol{i}\rangle$ respectively denoted normalised quantum representations of $\boldsymbol{v}(t)$ and $\boldsymbol{i}(t)$ defined on $\lceil \log_2(N) \rceil$ qubits:

$$|\boldsymbol{i}\rangle = \frac{\sum_k i_k|k\rangle}{\|\sum_k i_k|k\rangle\|_2}, |\boldsymbol{v}\rangle = \frac{\sum_k v_k|k\rangle}{\|\sum_k v_k|k\rangle\|_2}$$

where $|k\rangle$ represents the computational basis ($k = 1, \ldots, N$); i_k and v_k are the k^{th} element of $\boldsymbol{i}$ and $\boldsymbol{v}$, respectively.

Equation (2) embeds EMTP into Hilbert space. Therefore, any operators on (2) will be of exponential dimension. A silent feature of (2) is that $\boldsymbol{G}$ is sparse and symmetrical,[1] meaning its eigenvalues are real and its eigenvectors can form an orthonormal basis. Decompose $\boldsymbol{G}$ in its eigenbasis:

$$\boldsymbol{G} = \sum\nolimits_j \lambda_j |\boldsymbol{u}_j\rangle\langle\boldsymbol{u}_j| \tag{3}$$

[1]For non-Hermitian matrices, the algorithm still applies by augmenting the formulation as: $\begin{bmatrix} \boldsymbol{0} & \boldsymbol{G} \\ \boldsymbol{G}^\dagger & \boldsymbol{0} \end{bmatrix}\begin{bmatrix} \boldsymbol{0} \\ \boldsymbol{v} \end{bmatrix} = \begin{bmatrix} \boldsymbol{i} \\ \boldsymbol{0} \end{bmatrix}$. Consequently, the result is obtained by extracting the lower-half entries.

Manuscript received November 7, 2020; revised February 8, 2021; accepted March 6, 2021. Date of publication March 18, 2021; date of current version June 18, 2021. This work was supported in part by the Advanced Grid Modeling Program under Department of Energy's Office of Electricity, in part by the National Science Foundation under Grants ECCS-2018492 and OIA-2040599, in part by Stony Brook University's Office of the Vice President for Research through a Quantum Information Science and Technology Seed Grant, and in part by the Oak Ridge Leadership Computing Facility, which is a DOE Office of Science User Facility supported under Contract DE-AC05-00OR22725. Paper no. PESL-00313-2020. *(Corresponding author: Peng Zhang.)*

The authors are with the Department of Electrical and Computer Engineering, Stony Brook University, Stony Brook, NY 11794 USA (e-mail: yifan.zhou.1@stonybrook.edu; fei.feng@stonybrook.edu; p.zhang@stonybrook.edu).

Color versions of one or more figures in this article are available at https://doi.org/10.1109/TPWRS.2021.3067207.

Digital Object Identifier 10.1109/TPWRS.2021.3067207

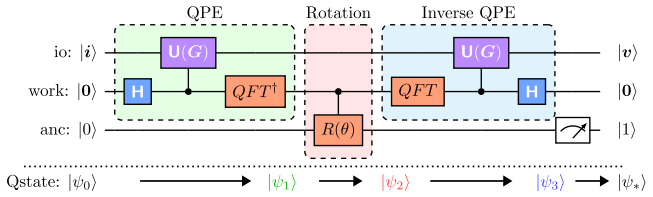

Fig. 1. Schematic diagram of HHL-based QEMTP circuit.

where $(\lambda_j, \boldsymbol{u}_j)$ are the j^{th} eigenpair of $\boldsymbol{G}$.

Similarly, $|\boldsymbol{i}\rangle$ is also decomposed in the eigenbasis of $\boldsymbol{G}$:

$$|\boldsymbol{i}\rangle = \sum\nolimits_j b_j |\boldsymbol{u}_j\rangle \tag{4}$$

Combining (3) and (4) yields the quantum-based solution:

$$\begin{aligned} |\boldsymbol{v}\rangle = \boldsymbol{G}^{-1}|\boldsymbol{i}\rangle &= \left(\sum\nolimits_j \lambda_j^{-1}|\boldsymbol{u}_j\rangle\langle\boldsymbol{u}_j|\right)\left(\sum\nolimits_j b_j|\boldsymbol{u}_j\rangle\right) \\ &= \sum\nolimits_j \lambda_j^{-1} b_j |\boldsymbol{u}_j\rangle \end{aligned} \tag{5}$$

Based on (2)-(5), the next step is to build proper quantum circuits to execute above functionality in Hilbert space, which will be detailed in Section III.

Algorithm 1: Quantum EMTP Algorithm.

▷ ***Initialization***: t_{array}, Δt, $\xi_{\max}$, $\boldsymbol{G}$, $\boldsymbol{i}_h(t)$;
for $t \in t_{array}$ **do**
  if *Power network changes* **then**
    Update $\boldsymbol{G}$, $\boldsymbol{i}_s(t)$;
  end
  Prepare $\boldsymbol{i} = \boldsymbol{i}_h(t) + \boldsymbol{i}_s(t)$, $\boldsymbol{v}_* = \boldsymbol{0}$, $\xi = 2\xi_{\max}$, $k = 0$;
  while *1* **do**
    ▷ ***HHL-based EMTP solving***:
    Prepare quantum registers io, w and a;
    Execute QPE, rotation and inverse QPE successively;
    Output $|\boldsymbol{v}\rangle = |\psi_*\rangle$ by (9);
    Quantum state tomography $|\boldsymbol{v}\rangle \longrightarrow \boldsymbol{v}$;
    Update $\boldsymbol{v}_* = \boldsymbol{v}_* + \boldsymbol{v}$;

    ▷ ***HHL Error Compensation***:
    Compute HHL error $\xi = \|\boldsymbol{G}\boldsymbol{v} - \boldsymbol{i}\|_2$, $k = k + 1$;
    if $\xi < \xi_{\max}$ ***or*** $k \geq Iter_{\max}$ **then**
      break;
    end
    Update $\boldsymbol{i} = \boldsymbol{i} - \boldsymbol{G}\boldsymbol{v}$;
  end
  Update result array $\boldsymbol{v}_{array} = \{\boldsymbol{v}_{array}, \boldsymbol{v}_*\}$;
end
▷ ***Output***: time-series nodal voltages $\boldsymbol{v}_{array}$;

III. Quantum EMTP Algorithm

A. HHL-Based QEMTP Solver

This subsection devises an HHL-based QEMTP solver (see Fig. 1). Three quantum registers are adopted, i.e., io for storing nodal current inputs and nodal voltage outputs, w for working on QEMTP equations, and a for storing ancilla qubits.

At each time step, $\boldsymbol{i}$ is updated to initialize $|\psi_0\rangle = |\boldsymbol{i}\rangle_{io} \otimes |\boldsymbol{0}\rangle_w \otimes |\boldsymbol{0}\rangle_a$. Then, three steps are carried out [4]:

- *Quantum Phase Estimation (QPE)*, which estimates the eigenvalues of $\boldsymbol{G}$ with an operator $U = e^{i\boldsymbol{G}\tau}$:

$$|\psi_1\rangle = \left(\sum\nolimits_j b_j |\boldsymbol{u}_j\rangle_{io}|\lambda_j\rangle_w\right) \otimes |\boldsymbol{0}\rangle_a \tag{6}$$

  where $|\psi_1\rangle$ is the quantum state after going through QPE; $|\lambda_j\rangle$ is the qubit representation of the j^{th} eigenvalue of $\boldsymbol{G}$.
- *Controlled Rotation*, which rotates register a with a specific angle conditioned on $|\lambda\rangle_w$ to produce a normalised state:

$$|\psi_2\rangle = \sum_j b_j |\boldsymbol{u}_j\rangle_{io}|\lambda_j\rangle_w \left(\sqrt{1-\frac{C^2}{\lambda_j^2}}|0\rangle + \frac{C}{\lambda_j}|1\rangle\right)_a \tag{7}$$

- *Inverse QPE*, which compiles register w to $|\boldsymbol{0}\rangle_w$ to uncompute the quantum states so that the final solution can be obtained by postselecting $|1\rangle$ on register a:

$$|\psi_3\rangle = \sum_j b_j |\boldsymbol{u}_j\rangle_{io} \left(\sqrt{1-\frac{C^2}{\lambda_j^2}}|0\rangle + \frac{C}{\lambda_j}|1\rangle\right)_a \tag{8}$$

$$|1\rangle_a |\psi_*\rangle \underset{\Longrightarrow}{} \sum_j \lambda_j^{-1} b_j |\boldsymbol{u}_j\rangle_{io} \approx |\boldsymbol{v}\rangle \tag{9}$$

Consequently, the HHL algorithm outputs the nodal voltages $\boldsymbol{v}$ on the quantum register io. HHL theoretically provides an exponential enhancement in computational complexity compared with its classical counterparts. From the space complexity perspective, QEMTP formulation in the Hilbert space only employs $\lceil \log_2(N) \rceil$ qubits to describe a N-dimensional vector, which is a logarithmic reduction. From the time complexity perspective, HHL runs at $\mathcal{O}(\log(N))$ [5], while the best general-purpose classical algorithm (i.e., the conjugate-gradient algorithm) runs at $\mathcal{O}(N)$.

B. Enhanced QEMTP

HHL aims at approximating $|\boldsymbol{v}\rangle$ by a quantum superposition, as detailed in (9), with the following stopping criteria [5]:

$$\text{Prob}(\||\hat{\boldsymbol{v}}\rangle - |\boldsymbol{v}\rangle\|_2 \leq \epsilon) > 0.5 \tag{10}$$

where ϵ is a desired error; $|\hat{\boldsymbol{v}}\rangle$ represents final quantum state to be output; Prob denotes probability. Restricted by the qubits resources, depth of quantum circuits and noise on quantum computers, an executable error for the HHL quantum circuit may lead to growing errors or even divergence during the step-by-step QEMTP calculation. To tackle the challenge, we revise the HHL algorithm to effectively mitigate the error accumulation, as follows.

Denote the quantum state tomography of $|\boldsymbol{v}\rangle$ as $\boldsymbol{v}$. Then, $\boldsymbol{v}$ is modified with $\Delta\boldsymbol{v}$ depending on the HHL error:

$$\boldsymbol{G}\Delta\boldsymbol{v} = \boldsymbol{i} - \boldsymbol{G}\boldsymbol{v} \tag{11}$$

Because (11) has an identical form as (1), HHL is then recursively executed to solve $\Delta\boldsymbol{v}$ until a satisfactory precision is reached. **Algorithm 1** summarizes the QEMTP procedure.

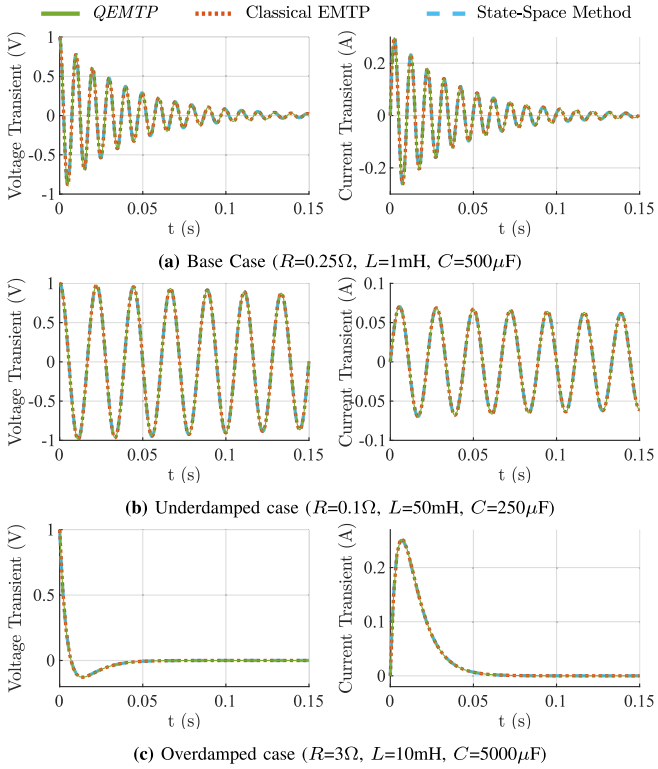

(a) Base Case (R=0.25Ω, L=1mH, C=500μF)

(b) Underdamped case (R=0.1Ω, L=50mH, C=250μF)

(c) Overdamped case (R=3Ω, L=10mH, C=5000μF)

Fig. 2. QEMTP results of RLC series circuit.

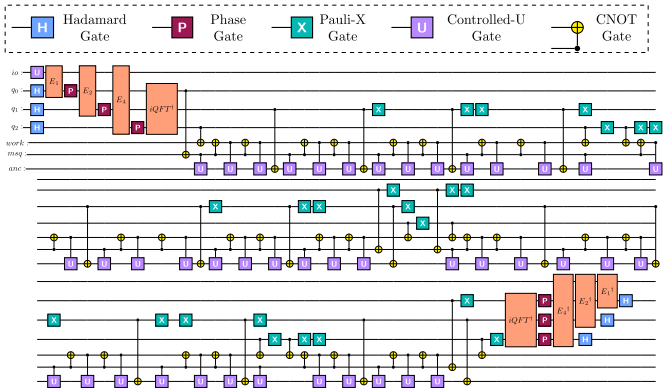

Fig. 3. Quantum circuit for base case of RLC series circuit (width: 7; depth: 102; number of CNOT gates: 54).

IV. Case Study

A. Validity of QEMTP

QEMTP is implemented in IBM Qiskit [6] and is verified first on a RLC series circuit switching into a DC source. Fig. 2 shows that QEMTP produces accurate electromagnetic results for the base case, underdamped case and overdamped case. The perfect match with those results from both classical EMTP and state-space approach verifies the effectiveness of QEMTP. The quantum circuit for the base case is illustrated in Fig. 3.

Fidelity, as defined below, is a preferred metric to measure the similarity of quantum states:

$$F(\rho_1, \rho_2) = [Tr\sqrt{\sqrt{\rho_1}\rho_2\sqrt{\rho_1}}]^2 \tag{12}$$

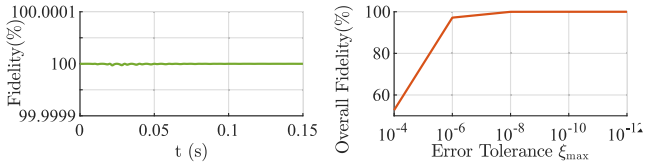

(a) Fidelity against classical EMTP **(b)** Tendency of fidelity with ξ_{max}

Fig. 4. QEMTP fidelity of RLC series circuit.

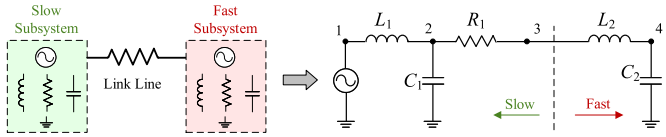

Fig. 5. Illustration of latency test system.

TABLE I
Latency System Parameters

R_1	L_1	C_1	L_1	C_1	f
2Ω	1mH	1μF	0.01mH	1μF	60Hz

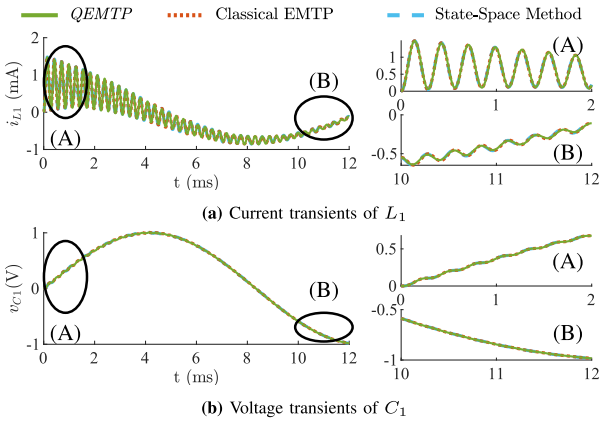

(a) Current transients of L_1

(b) Voltage transients of C_1

Fig. 6. QEMTP results of the latency circuit.

Therefore, we use fidelity to quantify the precision of QEMTP. As shown in Fig. 4(a), the fidelity between QEMTP and classical EMTP is consistently above 99.9999%, exhibiting the accuracy of QEMTP in performing electromagnetic simulations. Meanwhile, a flat fidelity curve also indicates that QEMTP effectively mitigates the inherent error accumulation in HHL. Fig. 4(b) further illustrates that reducing the error threshold ξ_{max} improves the accuracy of the QEMTP results.

B. QEMTP Application in a Latency Network

Since a common feature of power systems is the co-existence of fast-slow dynamics, QEMTP is further applied to a typical latency test system in [7] as an abstraction of the fast-slow dynamic systems (see Fig. 5). Table I presents the test system parameters.

QEMTP results show that the electromagnetic transients follow a fundamental frequency (60 Hz) carrier superimposed with high-frequency components. Fig. 6 also shows that the QEMTP results match those from the classical EMTP and state-space approach, further verifying the capability of QEMTP in handling

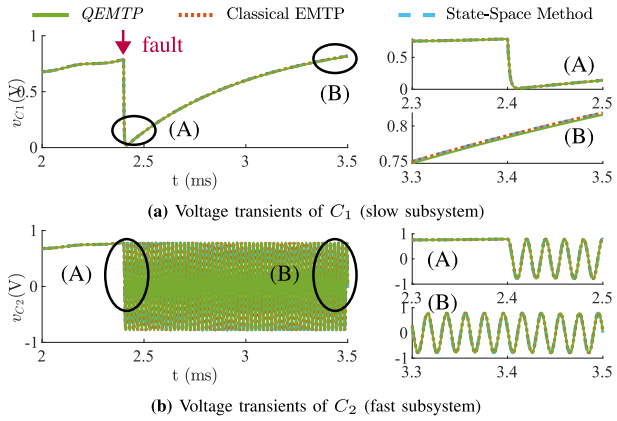

(a) Voltage transients of C_1 (slow subsystem)

(b) Voltage transients of C_2 (fast subsystem)

Fig. 7. QEMTP results of the latency circuit under a short-circuit fault.

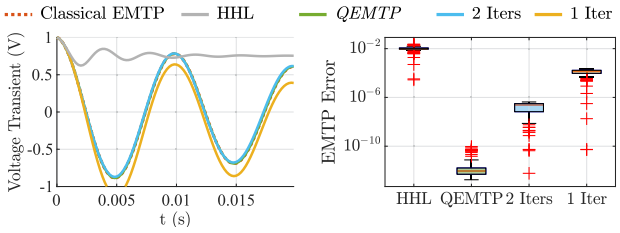

(a) EMTP results under different $Iter_{\max}$ **(b)** Precision under different $Iter_{\max}$

Fig. 8. Efficacy of error compensation in QEMTP.

the complicated fast-slow dynamics. Specifically, the zoomed view during the starting period (the most oscillating period) shows QEMTP's satisfactory performance in capturing the fast dynamics, while the zoomed plot for the final stage shows QEMTP's capability in mitigating the error accumulation.

Further, QEMTP is tested through the analysis of a large disturbance case. With a short-circuit fault occurred at bus 3 at 2.4 ms, the latency circuit is virtually split into a fast subsystem and a slow subsystem, which is coincident with the QEMTP results in Fig. 7. Moreover, Fig. 7(b) shows that QEMTP accurately captures the ultra-fast oscillations of the fast subsystem initiated by a large disturbance.

C. Further Discussion

To achieve high fidelity and robustness in a step-by-step EMTP, QEMTP enhances HHL with an error compensation technique, as detailed in Subsection III-B. Fig. 8 shows that, while QEMTP accurately matches the classical EMTP results, simply applying HHL to EMTP without error compensation suffers from severe error accumulation and fails to provide accurate transient trajectories after several timesteps. As a rule of thumb, QEMTP takes a slight effort of 2–4 iterations to satisfy the accuracy requirement of EMTP.

Although QEMTP is successfully prototyped, its real-world application is still restricted by today's quantum hardware, which is a common obstacle in this Noisy Intermediate-Scale Quantum (NISQ) era [8]. The execution of multiple shots for

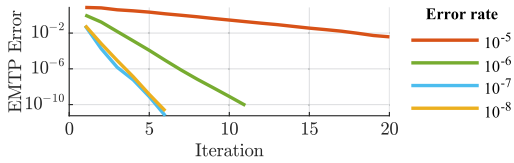

Fig. 9. Impact of noisy quantum environment on QEMTP's performance.

circuit measurement often hinders transforming the superior efficiency of quantum algorithms from theory to reality at the moment. Unavoidable noise and short coherence time also disturb the accuracy of quantum circuits. Fig. 9 briefly investigates QEMTP's performance in noisy quantum environment based on IBM QasmSimulator. QEMTP indeed exhibits certain tolerance of noise with the assist of error compensation, while HHL never survives under noisy environment. However, with a larger noise, QEMTP still suffers slow convergence. Our ongoing work is to enhance QEMTP's applicability in NISQ era by developing a hybrid quantum-classical QEMTP.

V. Conclusion

This letter is the first attempt to exploit the quantum computing capabilities in power system transient analysis. A quantum-enabled EMTP formulation is established, and an HHL-based QEMTP algorithm is devised. A revised HHL is devised to achieve a trade-off between high precision and limited quantum resource. Test results from a RLC circuit and a fast-slow dynamic system verify the correctness and efficacy of QEMTP. Even though the practicality of QEMTP is still restricted by availability of quantum resources, condition number of conductance matrix, executable depth of quantum circuit and noise of quantum computers [9], QEMTP opens a door to the development of numerous quantum grid analytics.

References

[1] H. W. Dommel, *EMTP Theory Book*, 2nd ed. Vancouver, BC, Canada: Micro Tran Power Syst. Anal. Corp., 1996.
[2] P. Zhang, W. Krawec, J. Liu, and P. Krstic, ASCENT: Quantum grid empowering a resilient secure power grid through quantum eng. Proposal# 2023915, *Nat. Sci. Found.*, Feb. 2020.
[3] J. D. Hidary, *Quantum Computing: An Applied Approach*. Berlin, Germany: Springer, 2019.
[4] A. W. Harrow, A. Hassidim, and S. Lloyd, "Quantum algorithm for linear systems of equations," *Phys. Rev. Lett.*, vol. 103, no. 15, 2009, Art. no. 150502.
[5] D. Dervovic, M. Herbster, P. Mountney, S. Severini, N. Usher, and L. Wossnig, "Quantum linear systems algorithms: A primer," 2018, *arXiv:1802.08227*.
[6] H. Abraham, AduOffei, and R.Agarwal, *et al.* "Qiskit: An open-source framework for quantum computing," 2019.
[7] J. A. Hollman and J. R. Marti, "Step-by-step eigenvalue analysis with emtp discrete-time solutions," *IEEE Trans. Power Syst.*, vol. 25, no. 3, pp. 1220–1231, Aug. 2010.
[8] J. Preskill, "Quantum computing in the NISQ era and beyond," *Quantum*, vol. 2, p. 79, 2018.
[9] S. Aaronson, "Read the fine print," *Nature Phys.*, vol. 11, no. 4, pp. 291–293, 2015.